Simulation studies of non-neutral plasma equilibria in an electrostatic trap with a magnetic mirror

K. Gomberoff, J. Fajans, and J. Wurtele
Center for Beam Physics, Lawrence Berkeley National Laboratory
and
Department of Physics, UC Berkeley
Berkeley CA 94720

A. Friedman, D. P. Grote, and R. H. Cohen
Fusion Energy Program, Lawrence Livermore National Laboratory
Livermore, CA 94550

J-L. Vay
Lawrence Berkeley National Laboratory
Berkeley CA 94720

The equilibrium of an infinitely long, strongly magnetized, non-neutral plasma confined in a Penning–Malmberg trap with an additional mirror coil has been solved analytically [J. Fajans, Phys. Plasmas **10**, 1209 (2003)] and shown to exhibit unusual features. Particles not only reflect near the mirror in the low field region, but also may be weakly trapped in part of in the high field region. The plasma satisfies a Boltzmann distribution along field lines; however, the density and the potential vary along field lines. Some other simplifying assumptions were employed in order to analytically characterize the equilibrium; for example the interface region between the low and high field regions was not considered. The earlier results are confirmed in the present study, where two-dimensional particle-in-cell simulations are performed with the Warp code in a more realistic configuration with an arbitrary (but physical) density profile, realistic trap geometry and magnetic field. A range of temperatures and radial plasma sizes are considered. Particle tracking is used to identify populations of trapped and untrapped particles. The present study also shows that it is possible to obtain local equilibria of non-neutral plasmas using a collisionless PIC code, by a scheme that uses the inherent numerical collisionality as a proxy for physical collisions.

I. INTRODUCTION

The equilibrium of a non-neutral plasma in a Penning-Malmberg trap has been the subject of many studies.[1,2,3] A mirror field has been suggested to cause transport in such traps[1]. Thermal equilibrium in Malmberg-Penning traps has been studied[4], but without a detailed analysis of mirror fields. A hollow electron column with axial mirrors has also been considered[5]. Penning-Malmberg traps have been recently used in experiments for the production of anti-hydrogen[6,7] and are considered, with mirror fields added to confine the anti-hydrogen itself, for future experiments as well [8,9].

Recently the effects of a multipole magnetic field intended to trap the anti-hydrogen radially in such a trap have been studied experimentally[10], theoretically[11], and with simulations.[12-13] This work was conducted at UC Berkeley as part of the ALPHA[8] collaboration. Future ALPHA experiments will use a mirror field. The results presented here are not meant to study the ALPHA geometry, but, rather are motivated by the study of how the non-neutral plasma equilibrium self-consistently changes as the mirror field is applied.

These numerical studies are motivated in part by earlier work[14], where it was shown analytically that a non-neutral plasma exhibits unusual features when a magnetic mirror field is added to the longitudinal field of the trap. In contrast to neutral plasmas, the density and potential along field lines is not constant. There are two trapping regions, one in the low field side and one in the high field side. Assuming that the velocity distribution is a Maxwellian, the density distribution obeys the Boltzmann relation (written for positrons),:

$$n(z;r_L) = n(z_L;r_L)\exp\left(\frac{-e\Delta\phi(z,r_L)}{kT}\right). \qquad (1)$$

Here $n = n(z;r_L)$ is the density value in along a field line originating at a radius r_L in the low field region, and $n(z_L;r_L)$ is the corresponding low field density. The potential difference along the same field line is $\Delta\phi(r;z_L) = \phi(r;z_L) - \phi(z_L;r_L)$.

A typical trap configuration is shown in Fig. 1.

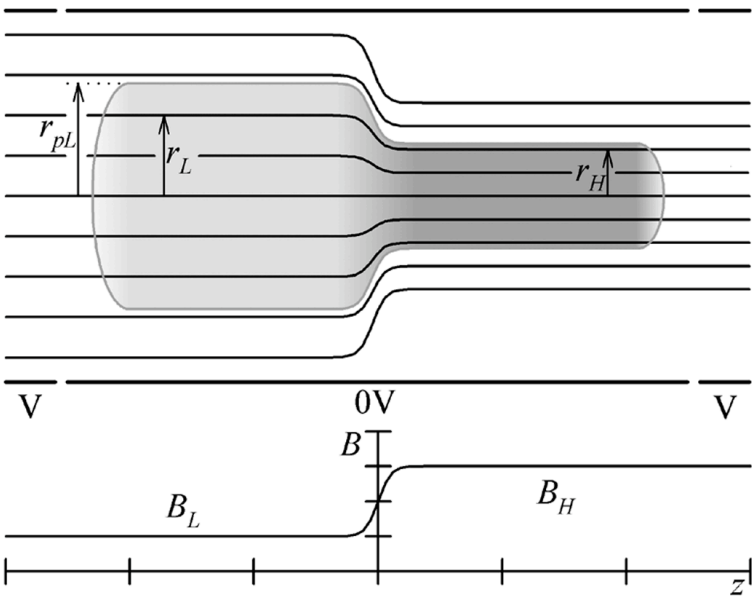

Fig. 1: Typical Penning-Malmberg trap with a mirror field. The magnetic field strength and field lines of the mirror are plotted as well as the plasma profile.

In Ref. 14, an infinitely long plasma is assumed and the transition between the high field and low field region is idealized via the conservation of magnetic moment. Additional assumptions were made in Ref. 14 in order to analytically characterize the equilibrium: the field variation was assumed small and a flat-top density profile was considered. Numerical solutions in the same paper[14] extend those results to broader regimes, however still considering an infinite plasma and ignoring the transition region between high and low field. In this paper we study plasma equilibria in a realistic two-dimensional geometry with finite plasma lengths and realistic magnetic field variations. We use the WARP simulation code[15] with a two-dimensional field solver (r-z). Thus, the simplifications required for the analytical study are not required. The plasma density decreases radially towards the plasma boundary. Initially the plasma is loaded, following the technique described in Refs. 12-13, into an equilibrium distribution which satisfies Eq. 1 along field lines in an initially uniform axial field. The mirror field is then ramped slowly until it reaches the desired value. The plasma appears to be in a new equilibrium, whose properties we investigate in detail.

We show the existence of two trapping regions and examine the deviations from constant density and potential along field lines; the Boltzmann distribution is obtained all along the field lines, including in the transition region between the high and low field, which is ignored in Ref. 14.

We previously used the same code to simulate the positron confinement in a proposed anti-hydrogen trap with an octupole magnetic field for the radial trapping of the anti-hydrogen[12]. We found that a proper equilibrium can be achieved with the Warp code, although it does not take realistic collisions into account. We employ the same techniques as in Refs. 12-13, in order to find the positron/electron equilibrium in the Penning-Malmberg trap with a magnetic mirror. Thus we show that by using the scheme described above, a local unknown equilibrium (with a nonuniform field) can be found from the uniform field equilibrium with a collisionless PIC code, using the collisionallity of the method to facilitate relaxation of the system.

It is not clear that a Maxwellian distributions in PIC simulations should be obtained as the result of numerical collisions. Numerical effects such as non-conservation of energy, unrealistic fluctuation levels associated with the reduced particle number, finite size macroparticles with an effective shape influenced by the grid, etc., could lead to different results. Early work by Dawson[16] showed that the plasmas modeled in a simple class of particle codes exhibit relaxation toward a Maxwellian state, as a result of three-body interactions; however, because entropy is (in general) continuously generated in PIC codes, there is formally no steady state. A detailed discussion of relaxation and related effects can be found in Chapters 12 and 13 of Ref. 17. We intend to explore these issues more thoroughly in future work, where we hope to be able to employ the physically-correct number of particles along with fine zoning. In this paper we emplyed a limited number of macroparticles, and so deliberately enhanced the numerical collisional effects in order to achieve more rqapid damping; the Boltzmann distribution obtained as a result indicates that Maxwelization is obtained to a very large degree for the present simulation parameters.

The Warp code[15] was designed, originally, for heavy ion beam simulations. This is a three-dimensional Particle-In-Cell (PIC) code that considers the self electrostatic fields of the particles, together with many external magnetic and electric field elements. One

feature that makes Warp a very suitable code for the present simulations is that the time step can be larger than the gyro period while the various drifts and Larmor radius are calculated properly[18]. Within these strongly magnetized plasmas, the motion is primarily determined by the guiding center dynamics. Another special feature of Warp is the Python-based user programmable ("steerable") capability that enables us to, for example, gradually turn on a mirror coil or add particles during the a simulation run.

The paper is organized as follows. In Section II the simulation set-up is described. In III we present the results for different plasma configurations, namely; plasmas of different density profiles and various temperatures. In IV we discuss the particle trapping. Finally, our conclusions are given in Section V.

II. SIMULATION GEOMETRY AND PARAMETERS

We describe here the set-up for the PIC simulations done with Warp. A representative simulation produces particles distributed in r-z as shown in Fig. 2. The trap geometry and parameters are apparent. Thus, the plasma is confined axially by two voltage rings of 100 V each. The plasma is confined radially by an axial magnetic field which, in the low field region, is 1T. The trap wall radius is 21 mm, the plasma column width at the high field region is 7 mm. The field is approximately a factor of 2.2 higher in the high field region due to the existence of a solenoid in the right half of the plasma. The plasma length is ~300 mm and the computational field grid's spacing is 1 mm. The time step for the simulation is $1 \cdot 10^{-10}$ s. The plasma density in the low field is of the order of $1 \cdot 10^{7}$ cm^{-3}; it decreases towards its radial boundary. The initial density distribution is loaded with the previousely calculated trap equilibrium. The particles have an initial Maxwellian velocity distribution. After computational equilibrium is obtained (following the technique described in Refs. 13), the mirror field is then ramped slowly (over several bounce times) until it reaches the desired value. We tracked the trajectories of selected particles; their motion along constant field lines was observed, allowing us to identify trapped particle regions and note their characteristic features

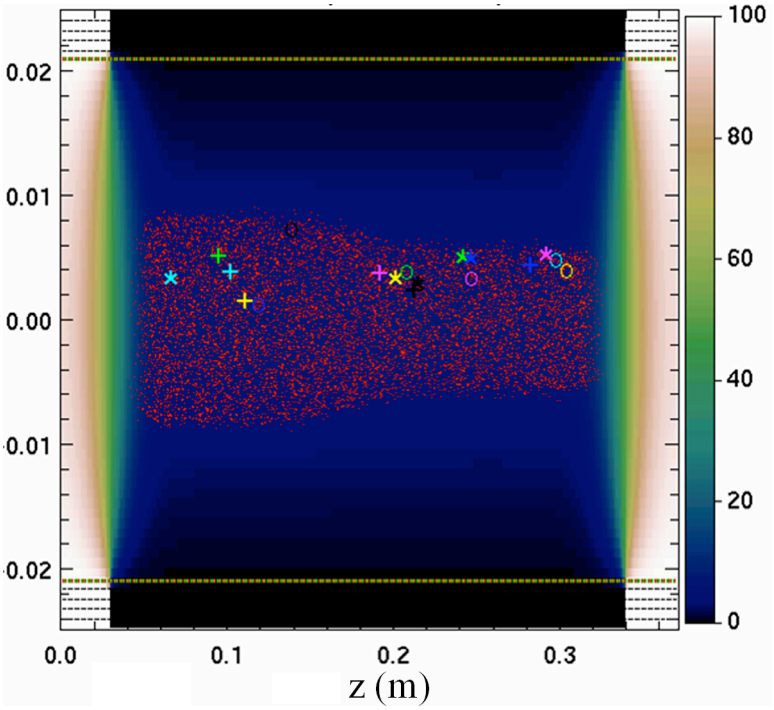

Fig. 2: Particles (and marked particles) in the Penning-Malmberg trap with a mirror field. The potential appears as a color map. Note that only a subset of the particles is shown, in order to prevent saturation. Trapped particle orbits were observed.

III. PARTICLE DISTRIBUTIONS

We here show the simulation results for various density profiles and plasma temperatures. The first case is for plasma temperature of 1 eV. For these parameters the Debye length is of the order of 2.5 mm. This length is much smaller than the plasma length and significantly smaller that the plasma radius.

In Fig. 3a we show a color map of the magnitude of the magnetic field, together with the corresponding field lines in the r-z plane. If B_L is the magnetic field in the low field value side, and B_H is the field at the high field side, then we define β via $B_H \equiv (1+\beta)B_L$. In this simulation $\beta \approx 1.2$. In Fig. 3b we show the density color map in the r-z plane and in Fig. 4a we show the value of the density on the axis. In the case of a cold, infinitely long plasma with an initially flat top density distribution and for for small Debye length compared to the wall radius the density should scale approximately with the field strength along the field line. [14] We can see from Fig. 3 that, in the interior of our plasma, for small

radii (where a flat-top and infinitely long plasma is a good approximation to our initial distribution) the density scales approximately as the magnetic field. On the axis the density in the high field region is ≈1.9 times the low region value. We can see that our density distribution increases along each field line over most of the plasma. In Figs. 4 and 5 we show the potential distribution. This result can appear at first sight as counterintuitive; however, the high-density region's outer radius is smaller than that of the low density region (due to the convergence of field lines), leading to a smaller potential than in the low field region, for the same field lines[14]. The potential decreases over most of the plasma region, and this is the reason that it is possible to obtain trapped particles in the high field region; they are reflected by the electrostatic potential as they move to lower field region. Along the axis, the potential decrease is of order 0.4V. However, at larger radii, there is a general trend for the potential variation along field lines to decrease. Along a field line that originates at a radius of ≈7±1 mm (marked with a dashed line in Fig. 5), the potential is constant and for larger radii it increases along field lines. We denote the field line with zero potential variation as the critical line; it defines a critical radius in both the high and in the low field regions. In the high field region particles cannot be trapped beyond the high field critical radius.

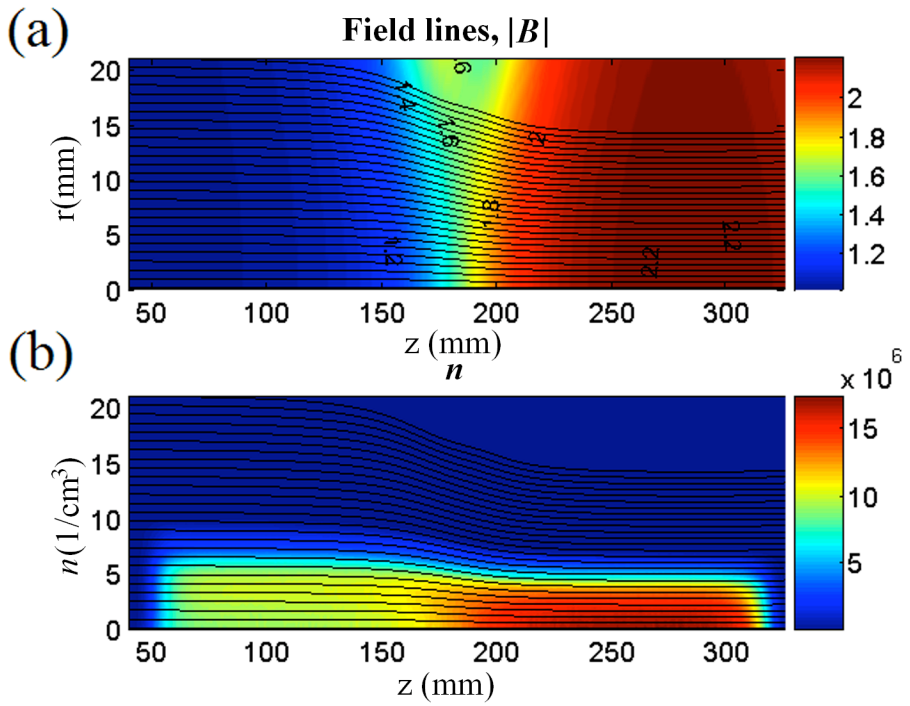

Fig. 3: (a) Color map of the magnetic field magnitude B (T) of the mirror field in the simulated non-neutral plasma trap. (b) Color map of the density (1/cm^3) and magnetic field lines for the case of a plasma at 1eV.

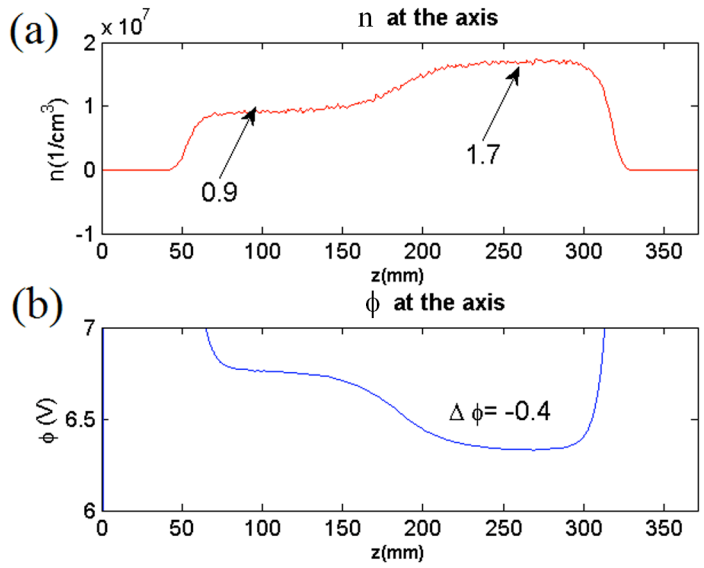

Fig. 4: (a) The density at the axis for the case of a plasma at 1eV. Averaged densities values in the low and high field region are shown (b) The potential at the axis for the same case.

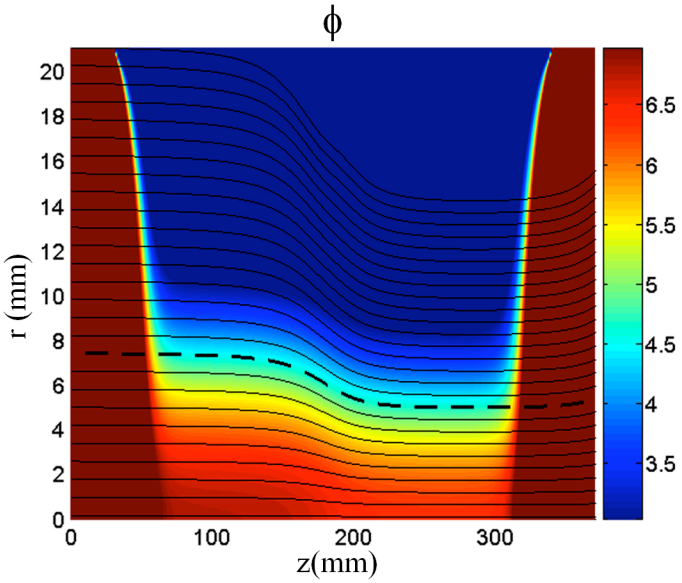

Fig. 5: Color map of the potential (V) and magnetic field lines for the case of a plasma at 1eV.

We evaluated the expression:

$$G(z;r_L) = \frac{n(r(z;r_L),z)}{n_L(r_L)\exp\left(\frac{-e\Delta\phi(r(z;r_L),z)}{kT}\right)} \quad , \tag{2}$$

where $\Delta\phi(r,z) = \phi(r,z) - \phi(r_L)$ on each field line, which is expected to be equal to 1. In Fig. 6 we show contour maps of G in the r_L-z plane. We have interpolated the different values over a finer grid, using the "Spline" function of Matlab. G is plotted in the region where the Boltzmann distribution is satisfied. Comparing with the density Fig. 3a, it appears that in our simulation the Boltzmann distribution is satisfied over most of the higher density region. i.e r_L<6 mm. The fact that in this simulation the Boltzmann distribution is not satisfied in the region of low densities, does not mean that the Boltzmann distribution is not satisfied there; rather, we believe that the results in this region are inaccurate. The main reason for this localized inaccuracy is that there are very few macroparticles here, resulting in very large numerical noise and heating. The effective temperature in this region is thus higher. The use of more macroparticles is an imperfect solution. Since the equilibration process is then slower in the high density region, the simulation time becomes much longer. This leads, in turn, to more heating in the high density region. Also a differential macroparticle charge could be used according to the density, leaving the number of particles per cell uniform. This could lead to other numerical problems due to particle mixing. Since we are mainly interested in the region of higher density, we did not attempt to develop the advanced numerics nor carry out the long simulations required to analyze the boundary regions in detail

In Ref. 14 the Boltzmann distribution was not solved for in the interface between the low and high density regions. Here, in the region where the Boltzmann distribution is shown to be satisfied, we show the expected result: the Boltzmann distribution is valid along field lines. We also remark that the values of G are not trivially uniform. If, for instance, $n_L(r_L)$ is replaced by $n_L(0)$, $G(z;r_L)$ can deviate significantly from unity over most of the plasma, also if the temperature is replaced by even slightly different values, this value deviates easily by a factor of several.

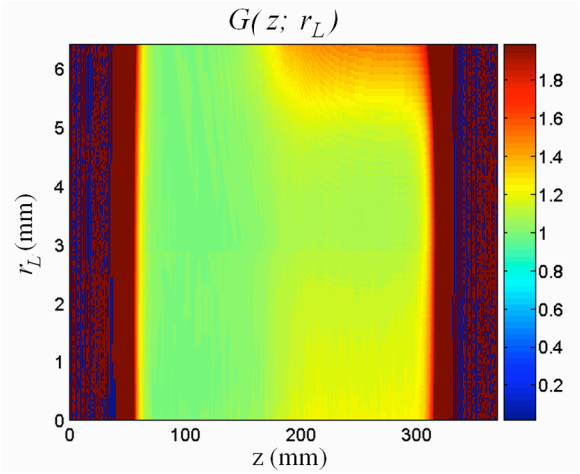

Fig. 6: Color map of $G(z;r_L)$ for the 1eV plasma. It should be noted that this is not a depiction of the physical r-z plane.

We also consider two cases with a larger plasma radius (14 mm). The first case has the same plasma density as before, and a temperature of 0.5 eV. For these parameters the Debye length is even smaller, about 1.7 mm. However, we still resolve it with the grid spacing in the high density region. The second case has a higher temperature (2eV). In Fig. 7 we show the initial density distribution for the 2eV case. The radial fall-off is clearly seen (the choice of radial profile is somewhat arbitrary).

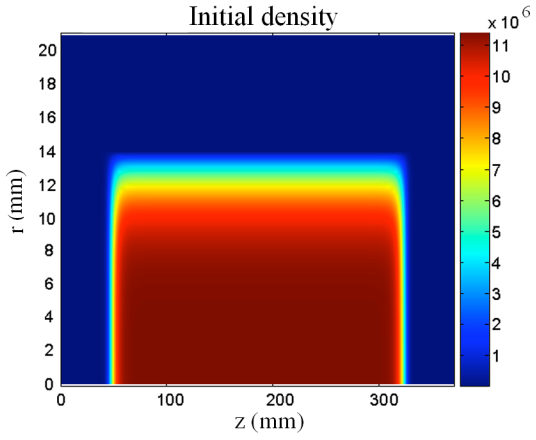

Fig. 7: Color map of the initial density distribution (1/cm^3).

For the 0.5eV temperature case, we expect that the density will scale as the field strength with even higher accuracy than for the higher temperatures. In Fig. 8a, we plot

the density color map and the field lines. In this case, the density on the axis is 2.05 times its value in the low field region, as can be seen from Fig. 9a. This is close to the 2.2 ideal value for a cold plasma. In Fig. 8b, we show the potential color map. We can see that the critical radius occurs at r_L=10±1 mm. The decrease of the potential on the axis is of order 0.3V (Fig. 9b).

In the case of a 2eV plasma, the density increase on the axis, as expected, is somewhat smaller than in the previous cases. The density is ≈1.8 times larger in the high field region than in the low field region (see Fig. 9a). The potential decrease along the axis is about 0.8V (Fig. 9b), higher than in the colder case. In Fig. 10a, the density color map is shown and in Fig. 10b the potential is plotted. We can see that the critical radius occurs at r_L=9±1 mm. Clearly, as the temperature decreases the transition between the density in the low and high field region occurs on a smaller scale.

In Fig. 11 we plot color maps of the function G in the r_L-z plane for both cases. We observe that the Boltzmann equation is satisfied over a similar region in both cases. This region is roughly within the critical radius. On the plasma boundaries, there is some numerical heating, so that a rough Boltzmann distribution is satisfied, but at an increased temperature. The somewhat discontinuous lines are due to the finite grid and the existence of numerical noise.

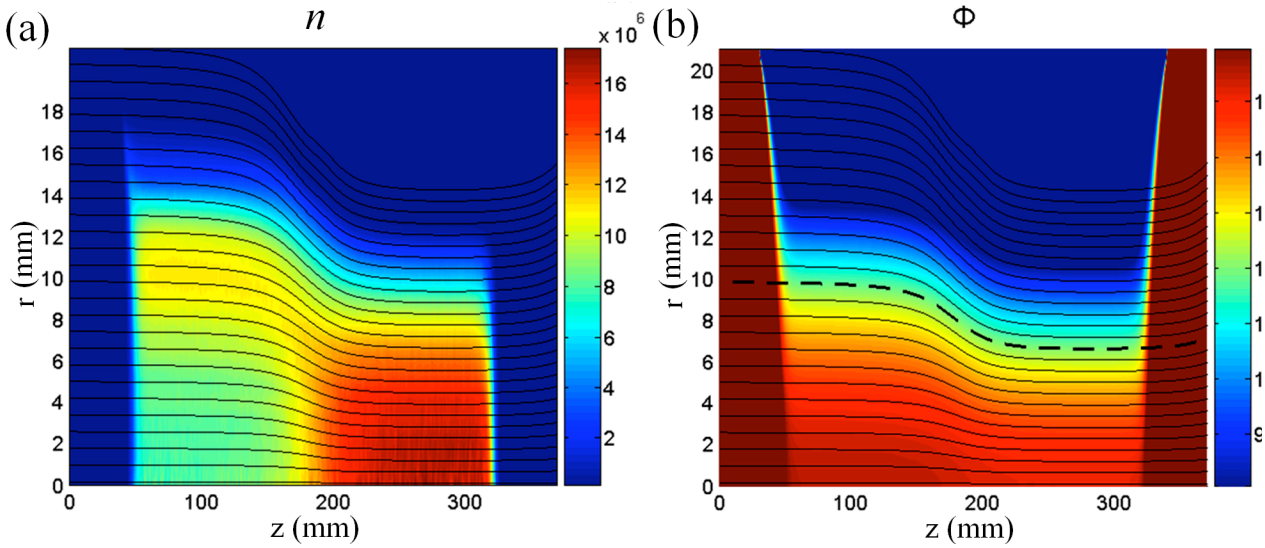

Fig. 8: (a) Color map of the density n (1/cm^3) and magnetic field lines for T=0.5 eV. (b) Color map of the potential ϕ(V) and magnetic field lines for the same plasma.

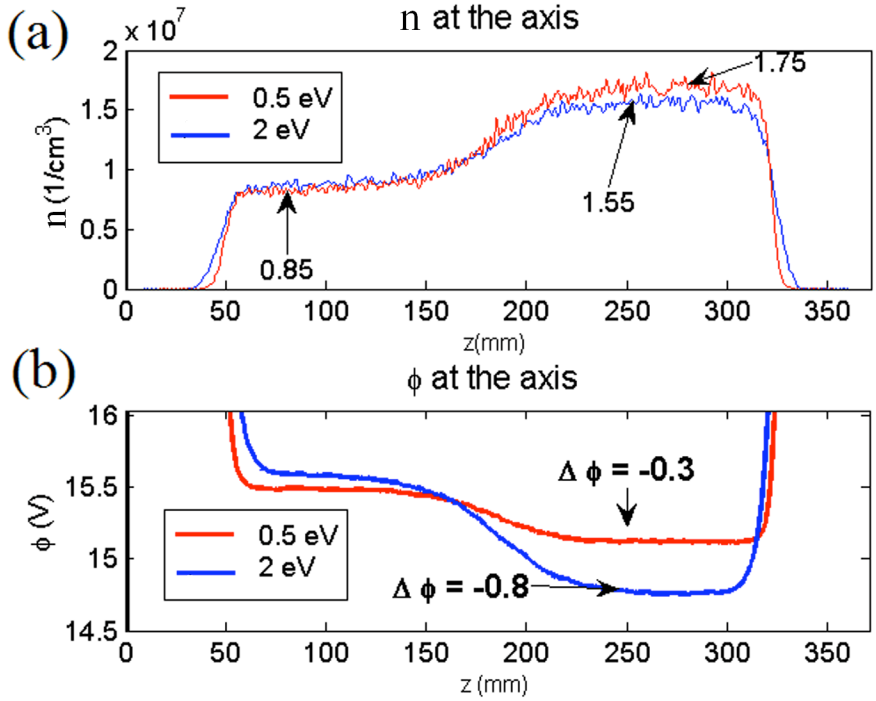

Fig. 9: (a) The density n (1/cm^3) and on axis, T= 0.5 eV (red) and T=2 eV (blue) cases. . Averaged densities values in the low and high field region are shown. (b) the potential ϕ(V) on axis for the same cases.

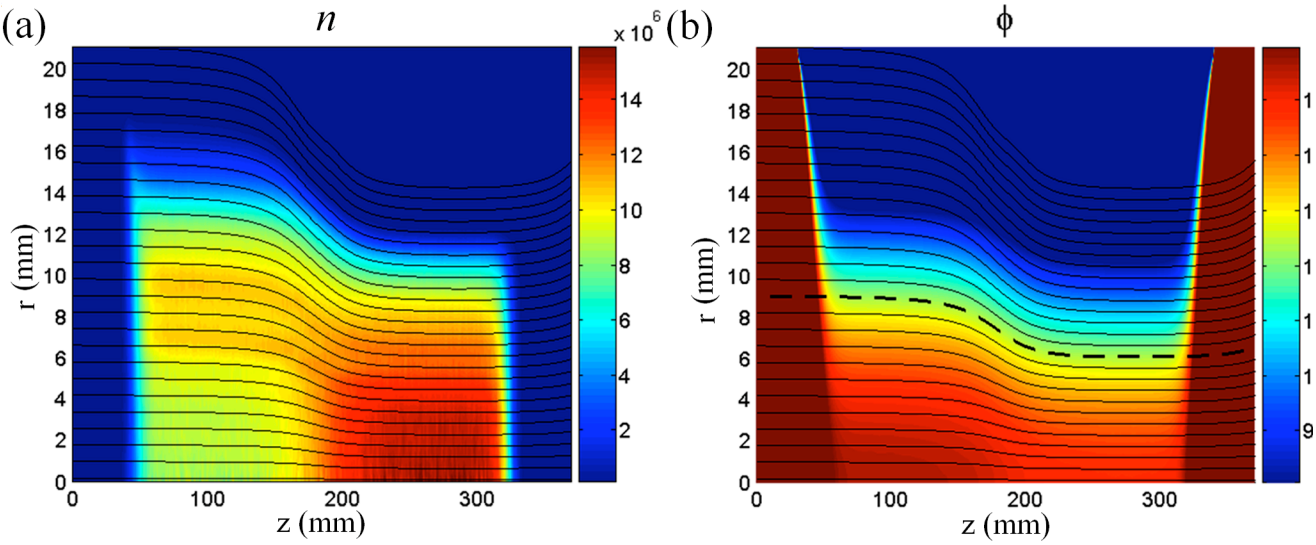

Fig. 10: (a) Color map of the density n (1/cm^3) and magnetic field lines for T=2.0 eV. (b) Color map of the potential ϕ(V) and magnetic field lines for the same plasma.

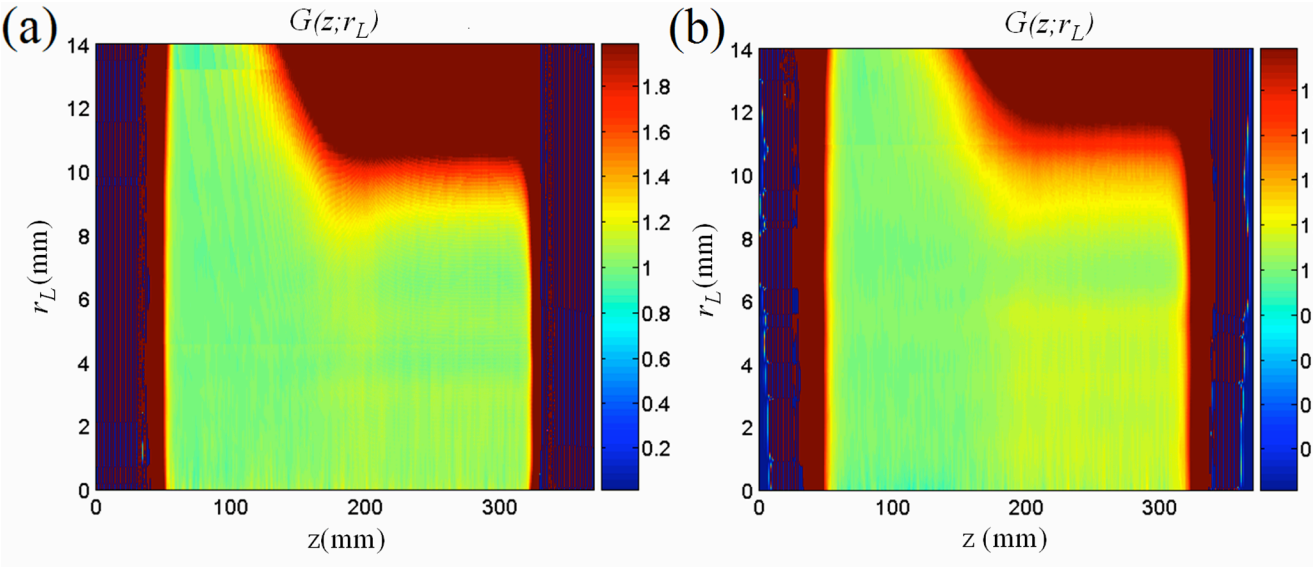

Fig. 11: Color map of $G(z;r_L)$ (defined in Eq. 2) for (a) T=0.5eV and (b) T=2.0eV.

IV. PARTICLE TRAPPING

The simulations show that some particles are trapped in the low field region, others (relatively few) are transiently trapped in the high field region, and most oscillate between the two potential barriers at the ends of the plasma. A typical untrapped particle trajectory is shown in Fig. 12. The axial position is plotted as function of time in Fig. 12a and the orbit in r-z is plotted in Fig. 12b (the orbit follows a field line).

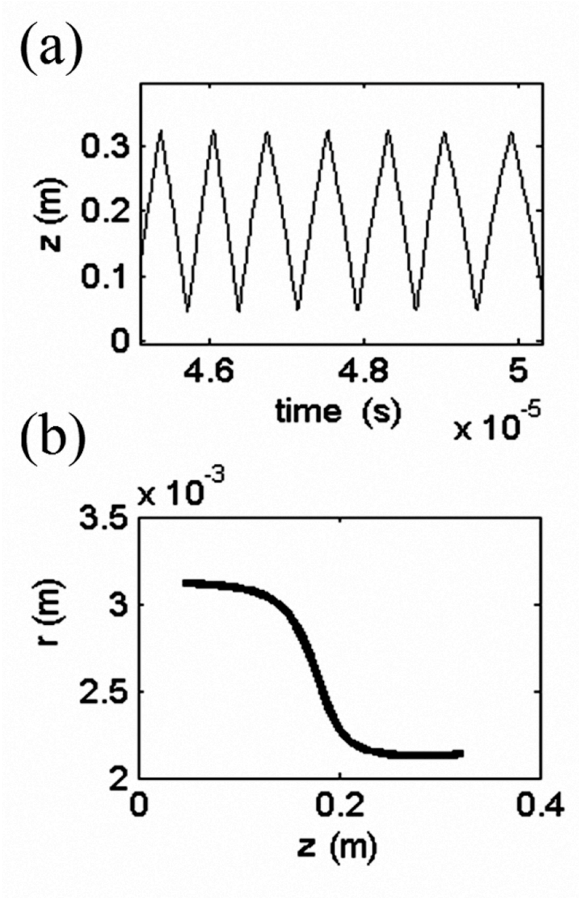

Fig. 12: Typical untrapped particle trajectory for a *T*=0.5eV plasma. (a) axial position as a function of time. (b) Particle trajectory in r-z plane.

Energy and magnetic momemt conservation yields[14] a useful expression in approximation where the plasma is long, and the transition region between the high and low fields and plasma boundary are neglected:

$$V_{\perp} = \sqrt{\frac{1}{\beta}\left(V_{||}^{2} - \frac{2e\Delta\phi}{kT}\right)} \tag{3}$$

Here $V_{\perp}, V_{||}$ are the transverse and axial velocities of the particles, respectively, normalized by the thermal velocity given by $V_T = \sqrt{kT/m}$. This gives a hyperbolic shape of the separatrix between the particles trapped in the low field region and those that are untrapped. For sufficiently large perpendicular velocities particles are trapped. In case where there is zero potential variation along the field lines the separatrices reduce to

the cold limit of straight lines originating at the origin. Thus, the trapping of particles is favored at larger radii, where the potential variation is smaller or even positive. At the smaller radii, the trapping is favored at lower temperatures since the potential difference is smaller. In our examples, the potential variation is, at most, of the order of 0.3-0.8 V (for the 0.5 eV - 2eV cases, respectively). For the potential term in Eq. 3, this gives a value of <0.6 in the 0.5 eV case and 0.8 in the 2 eV case. Since $\sqrt{\beta} \approx 1$, particles reflected in the low field region should have perpendicular velocity of at least the value of the parallel velocity (for radii lower than the critical radius). They can have lower values only for radii larger than the critical radius. These features are observed. There is large number of trapped particles in the low field region and more particles are trapped at larger radii (also as expected). A typical result for a trapped particle for a T=0.5 eV plasma is shown In Fig. 13a-b. The particle is inside the critical radius, therefore its perpendicular velocity should be larger than its parallel velocity. Indeed, the highest parallel velocity is $5 \cdot 10^5$ m/s, while the perpendicular velocity is at most $9 \cdot 10^5$ m/s. The particle follows a field line trajectory.

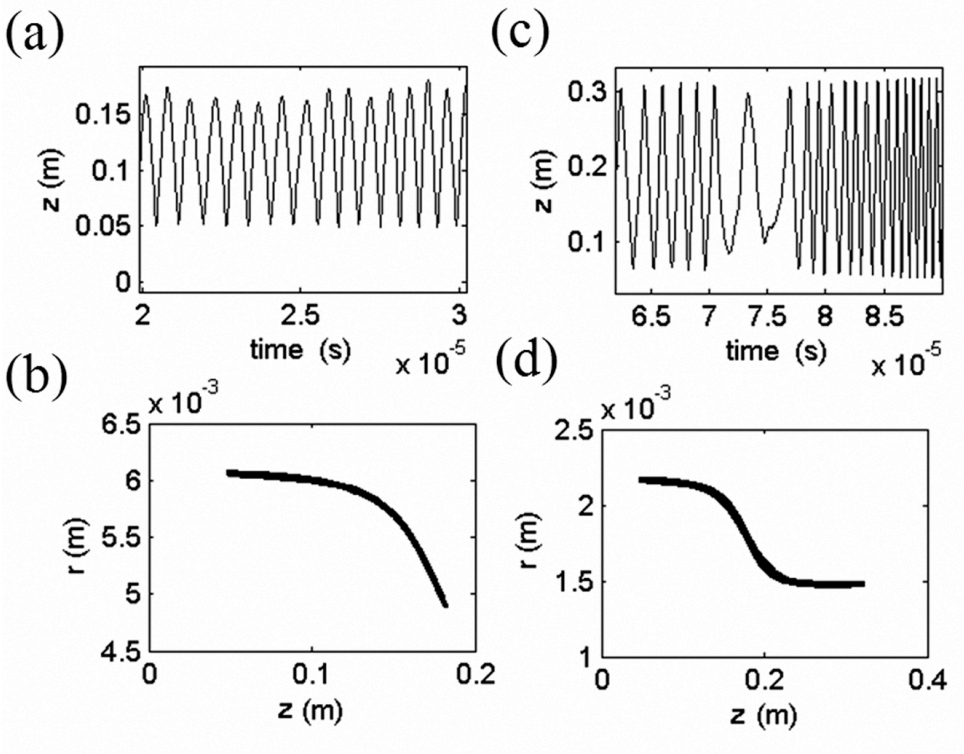

Fig. 13: Trapped particles trajectories. (a-b) a trapped particle orbit in the low field region in a *T*= 0.5eV plasma. (c-d) a particle is weakly trapped (for a few oscillations) in the high field region (*T*=1 eV). In (a) and (c) the axial position is plotted as function of time. In (b) and (d) the radial position versus the axial position are plotted.

In the high field region,

$$V_{\perp} = \sqrt{\frac{1+\beta}{\beta}\left(-V_{||}^{2} - \frac{2e\Delta\phi}{kT}\right)} \tag{4}$$

This yields an elliptical shape for the separatrices, which for the analytical top hat distribution decrease in size as the radius increases. For our parameters, the value of the second term is positive only for radii less than the critical, and is relatively large only for small radii (see, for example, the potential in the 1 eV case of Fig. 5). Thus, particles can be trapped in the high field region only if the parallel velocity is sufficiently small. In Fig. 13c-d we show a particle reflected while traversing from the high to low field region for the 1 eV plasma. In fact, this occurs near the origin, where the potential rise in the low

field region is highest. The parallel velocity of this particle is in fact small, $3 \cdot 10^{5-}$ m/s, giving rise to a positive term in the square root in Eq. 4.

We tracked the motion of a small number (18) of particles, with randomly chosen initial conditions consistent with the initial thermal distribution. Since particles can be de-trapped and trapped due to numerical collisions, the observed fraction (0.3-0.5) of trapped particles is only an estimate. This is consistent with the expected number of trapped particles in this region[14] ($\approx \sqrt{\beta/(\beta+1)}$ which is the value in the cold limit).

We observed only few particles that were trapped in the high field region (and they were trapped only for short times. This is expected to be a small fraction on the basis of the phase space analysis for the idealized case.

V. CONCLUSIONS

We have performed Warp simulations of two-dimensional plasma dynamics in a Malmberg trap with a mirror field. We use a technique to relax the simulated plasma to an equilibrium in a uniform field that was developed[13] for anti-hydrogen traps. We then ramp the mirror field and find numerical agreement with a basic theory that describes the equilibrium distribution in the mirror geometry. Thus, we show that the local equilibrium (with a nonuniform field) can be found from the uniform field equilibrium with a collisionless PIC code, as a consequence of the numerical noise. The Boltzmann distribution is shown to describe the plasma distribution along field lines. The density and potential need not be and are not constant along field lines. Moving beyond the earlier theory, the simulation shows that the Boltzmann distribution is satisfied in the transition region between the high and low fields. The unusual behavior of the non-neutral plasma, with some degree of trapping in both the high and low field regions, is demonstrated.

Acknowledgements: This work was supported by the US DOE Division of High Energy Physics, Grant number DE-FG02-04ER41289, and was performed under the auspices of the U.S Department of Energy by the University of California, Lawrence Livermore and Lawrence Berkeley National Laboratories under Contract Nos. W 7405-Eng-48 and DE-AC02-05.

[1] A. Kabantsev and C. Driscoll, Phys. Rev. Lett **89**, 245001 (2002).

[2] T. M. O'Neil and C. Driscoll, Phys. Fluids **22**, 266 (1979).

[3] S. A. Prasad and T. M. O'Neil, Phys. Fluids. **22**, 278 (1979).

[4] D. Dubin and T. M. O'Neil, Rev. Mod. Phys. **71**, 87 (1999).

[5] R Davidson, A. Drobot, and C A Kapetanakos, Phys. of Fluids **16**, 2199 (1973).

[6] M. Amoretti, C. Amsler, G. Bonomi, A. Bouchta, P. Bowe, C. Carraro, C. L. Cesar, M. Charlton, M. J. T. Collier, M. Dose et al. (ATHENA collaboration), Nature (London) **419**, 456 (2002).

[7] G. Gabrielse, N. S. Bowden, P. Oxley, A. Speck, C. H. Storry, J. N. Tan, M.Wessels, D. Grzonka, W. Oelert, G. Schepers,et al. (ATRAP Collaboration), Phys. Rev. Lett. **89,** 213401 (2002).

[8] W. Bertsche, A. Boston, P.D. Bowe, C.L. Cesar, S. Chapman, M. Charlton, M. Chartier, A. Deutsch, J. Dilling, J. Fajans et al. (ALPHA Collaboration), "The ALPHA Experiment: A Cold Anti-Hydrogen Trap", Prepared for International Conference on Low Energy Antiproton Physics (LEAP'05), Bonn, Juelich, Germany, 16-22 May 2005. Published in AIP Conf. Proc.796:301-308, 2005. Also in "Bonn 2005, Low energy antiproton physics" 301-308.

[9] W. Bertsche, A. Boston, P.D Bowe, C. L. Cesar, S. Chapman, M. Charlton, M. Chartier, A. Deutsch, J. Dilling, J. Fajans, (ALPHA collaboration) ,"A Magnetic trap for antihydrogen confinement", Submitted to NIMA (2006).

[10] J. Fajans, W. Bertsche, K. Burke, S. F. Chapman, and D. P. van der Werf, Phys. Rev. Lett. **95**, 155001 (2005).

[11] J. Fajans, A. Schmidt, Nucl. Instrum. Methods Phys. Res., Sect A **521**,318 (2004).

[12] K. Gomberoff, et al., "Warp Simulations of Anti-Hydrogen trap", To be submitted to Phys. Plasmas.

[13] K. Gomberoff, J. Fajans, J. Wurtele, D. Grote, J-L, Vay, A. Friedman. " Three Dimensional Simulations of Non-Neutral Plasmas Using Warp ", in preparation

[14] J. Fajans, Phys. Plasmas **10**, 1209 (2003).

[15] D. P. Grote, A. Friedman, I. Haber, J-L Vay, 2004 ECRIS Workshop, AIP Conf. Proc. **749**, 55, (2005).

[16] J. M. Dawson, "Thermal relaxation in a one-species, one- dimensional plasma," Phys. Fluids 7, 419-425, March 1964.

[17] C. K. Birdsall and A. B. Langdon, "Plasma Physics via Computer Simulation," McGraw-Hill, New York, 1985, Chap. 13.

[18] R. H. Cohen, A. Friedman, M. Kireeff Covo, S. M. Lund, A. W. Molvik, F. M. Bieniosek, P. A. Seidl, J.-L. Vay, P. Stoltz, and S. Veitzer, Phys. Plasmas **12**, 056708 (2005).